

TEC Depletion Generated by the Total Solar Eclipse of 2 July 2019

Julian Eisenbeis, Giovanni Occhipinti

▶ **To cite this version:**

Julian Eisenbeis, Giovanni Occhipinti. TEC Depletion Generated by the Total Solar Eclipse of 2 July 2019. Journal of Geophysical Research Space Physics, 2021, 126, 10.1029/2021JA029186 . insu-03589768

HAL Id: insu-03589768

https://insu.hal.science/insu-03589768

Submitted on 26 Feb 2022

HAL is a multi-disciplinary open access archive for the deposit and dissemination of scientific research documents, whether they are published or not. The documents may come from teaching and research institutions in France or abroad, or from public or private research centers.

L'archive ouverte pluridisciplinaire **HAL**, est destinée au dépôt et à la diffusion de documents scientifiques de niveau recherche, publiés ou non, émanant des établissements d'enseignement et de recherche français ou étrangers, des laboratoires publics ou privés.

Copyright

Check for updates

JGR Space Physics

RESEARCH ARTICLE
10.1029/2021JA029186

TEC Depletion Generated by the Total Solar Eclipse of 2 July 2019

Julian Eisenbeis[1] and **Giovanni Occhipinti**[1,2]

[1]Université de Paris, Institut de Physique du Globe de Paris, CNRS, Paris, France, [2]Institut Universitaire de France, Paris, France

Key Points:

- GNSS observations of solar eclipse show total electron content (TEC) depletions
- We observe TIDs of >200-km wavelength that are related to the TEC depletion due to the Moon's shadow
- Total solar eclipse proves robustness of the omega-k analysis

Correspondence to:

J. Eisenbeis,
julian.eisenbeis@irap.omp.eu

Citation:

Eisenbeis, J., & Occhipinti, G. (2021). TEC depletion generated by the total solar eclipse of 2 July 2019. *Journal of Geophysical Research: Space Physics*, *126*, e2021JA029186. https://doi.org/10.1029/2021JA029186

Received 27 JAN 2021
Accepted 2 DEC 2021

Abstract A total solar eclipse occurred at the ascending node of the Moon's orbit on 2 July 2019, with an eclipse magnitude of 1.0459. The totality was visible from the southern Pacific Ocean east of New Zealand to the Coquimbo Region (Chile) and Central Argentina at sunset, with the maximum of 4 min 32 s visible from the Pacific Ocean. The recent Great American Eclipse, 21 August 2017, clearly showed that the ionosphere is strongly affected by the totality. In order to explore the ionospheric signature of the 2019 eclipse, we use data of ∼110 GNSS stations seeing multiple GPS and GLONASS satellites to visualize the eclipse signature on the total electron content (TEC) in the southern hemisphere. The location of the South American GNSS stations, at the end of the path of totality, right before sunset, makes the eclipse signature in the ionospheric TEC act like an early sunset with 15 TEC-Unit variations, corresponding to 40% of background ionization. The effect reaches only four TEC-Units, corresponding to 25%–40% of background ionization, for the more westerly observations, where we clearly highlight the effect of the eclipse in the ionosphere and the following recovery to normality. By applying the omega-k analysis, we can find TIDs with wavelengths of around 100 km and larger than 200 km and with periods of 20–50 min, which supports the results of the Great American Eclipse. Using different grids, we can also prove the robustness of the omega-k analysis.

Plain Language Summary A total solar eclipse occurred on 2 July 2019 over the Pacific Ocean and South America with the eclipse shadow reaching the eastern coast of South America near Buenos Aires around sunset. We calculate the differential total electron content (TEC) to visualize the evolution of the phenomena with high spatial and temporal resolution. The effect of the eclipse in the ionosphere is clearly visible and appears as TEC depletion, which for some stations of central and eastern South America looks just like an early sunset. The omega-k analysis confirms the results of the Great American Eclipse regarding wavelength and period of the TIDs induced by the shadow of the Moon. Using different grids, we proved the robustness of the omega-k analysis. The effect of the solar eclipses in the southern hemisphere is coherent with the observations in the northern hemisphere even if we do not recognize the presence of bow waves.

1. Introduction

During the total solar eclipse of 2 July 2019, the Moon's shadow travels over the Pacific Ocean to the east coast of South America. It takes about 4 min for the shadow to cross the South American continent from Chile through Argentina where the last position of totality before sunset was near Buenos Aires. It also travels over a dense network of ∼110 GNSS stations giving the opportunity to analyze and explore the effect of the Moon's shadow in the southern ionosphere with high spatial resolution. The radical changing of the solar radiation due to the Moon's shadow produces a quick electron density decrease in the ionosphere, clearly visible in the total electron content (TEC) measured by GNSS stations. Indeed, the TEC represents the electron density integrated along the ray-path between the GNSS station and the satellite. The magnitude of the TEC depletion produced by the Moon's shadow was already studied in the past and was found to depend on the latitude (Le et al., 2009). Other studies confirmed this effect: for total solar eclipses the TEC depletion can reach 30–40% at midlatitudes with a delay of 5–20 min after the passing of the Moon's shadow (Ding et al., 2010; Jakowski et al., 2008), 10%–30% at high latitudes (Afraimovich et al., 1998; Hoque et al., 2016; Momani et al., 2010) whereas for the equatorial latitudes it can reach >40% due to the increased ionization within the equatorial anomaly (Tsai & Liu, 1999). The effect related to the latitude mainly depends on the elevation angle of the Sun and therefore higher ionization at low latitudes, which increases the background TEC and amplifies the effect of the solar eclipse.

© 2021. The Authors.
This is an open access article under the terms of the Creative Commons Attribution License, which permits use, distribution and reproduction in any medium, provided the original work is properly cited.

The 21 August 2017 solar eclipse over the US happened at midlatitudes like the South American eclipse of 2 July 2019 and, thanks to the high resolution coverage of the extensive North American network of roughly 3,000 GNSS stations, it was a great opportunity to confirm the presence of a TEC depletion and also to highlight the presence of traveling ionospheric disturbances (TIDs), some of them identified as bow waves and generated by the supersonic movement of the Moon's shadow (Cherniak & Zakharenkova, 2018; Coster et al., 2017; Eisenbeis et al., 2019; Sun et al., 2018). A simulation of bow waves during the eclipse (Lin et al., 2018) reproduced TIDs with a period of 20–30 min and therefore similar characteristics to the bow waves observed by Zhang et al. (2017).

Notwithstanding the TEC observations are firmly established, the different works in literature diverge about the physical origin of the propagating waves observed in the ionosphere. For instance, Mrak, Semeter, Drob, & Huba (2018) identify the origin of the TIDs as the EUV (extreme ultraviolet) modulation related to high energy sunspots instead of the Moon's shadow supersonic movement. In a following work, Mrak, Semeter, Nishimura, et al. (2018) found that thunderstorms are also an additional potential source of observed TIDs in addition to the EUV.

Eisenbeis et al. (2019) presented—for the first time—a complete omega-k analysis, based on a 3D Fast Fourier Transform, of the TEC variations observed by GNSS during the Great American solar eclipse to extensively highlight the main periods, wavelengths, and speeds of the observed waves and to separate the signatures of different observed waves. Eisenbeis et al. (2019) confirmed the presence of TIDs with period of 40–70 min and wavelength of 200–450 km observed and modeled by previous works (e.g., Coster et al., 2017; Lin et al., 2018; Sun et al., 2018; Zhang et al., 2017) and also confirmed the presence of the bow waves created by the supersonic movement of the Moon's shadow.

The analysis of the 2 July 2019 eclipse is a good occasion to explore the effect in the southern hemisphere and to compare it to the Great American Eclipse.

For instance, Jonah et al. (2020) investigated the effect of the eclipse of 2 July 2019 on the equatorial ionization anomaly (EIA) and found a 57% increase in TEC around the EIA crest as well as the expected 35% decrease in TEC south of the EIA in the path of the eclipse. They relate the TEC increase with an enhanced plasma fountain effect. Bravo et al. (2020) used ionosonde and GNSS TEC data to find a decrease in TEC in the area from 40°S to 30°S and an increase in TEC further north.

In this work, we present our analysis of the TEC depletion and we apply the omega-k analysis developed by Eisenbeis et al. (2019) to fully highlight the physical characteristics (wavelength and period) of the wave propagation.

2. Data and Methodology

In order to visualize the TEC perturbations induced by solar flux variations related to the total solar eclipse, we used a database consisting of 110 GNSS stations and capturing signals from GPS and GLONASS satellites. Using both GPS and GLONASS increases the number of available data by a factor of 1.5–2 compared to the use of GPS only. We use data from the freely available RAMSAC (Red Argentina de Monitoreo Satelital Continuo) network (Piñón et al., 2018) and stations in neighboring countries as Chile, Uruguay, or Brazil available through the UNAVCO web interface. Although the coverage is by far not as dense as for the Great American Eclipse, the affected area is covered fairly well by the network. The used ground-based stations continuously record data with a sampling rate of 30 s or higher. We only use data of satellite-station pairs with an elevation angle of >15°. To compute slant TEC (sTEC) we use the Spectre code (Lognonné et al., 2006) which we improved here to compute also GLONASS data additional to GPS.

The sTEC for each satellite-receiver pair is converted to vertical TEC (vTEC) for the height of the maximum ionization of the ionosphere, so it represents the vTEC directly above the receiver. For the conversion of slant TEC to vertical TEC, we use the following mapping function (Dautermann & Calais, 2008):

$$\mathrm{vTEC} = \mathrm{sTEC} * \sqrt{1 - \left(\frac{\cos(\theta) R_E}{R_E + h_I}\right)^2}$$

where θ is the satellite elevation angle, R_E is the mean radius of the Earth, and h_I is the height of maximum ionization in the ionosphere (here 300 km).

In order to compute the differential vTEC, we define the unperturbed background as the polynomial fit of eighth degree of our data. The differential vTEC for each receiver-satellite couple is computed separately.

For comparison of the effect of the eclipse with the surrounding days for single station-satellite pairs, we have computed absolute sTEC using the minimum scalloping method (Rideout & Coster, 2006) as described in Eisenbeis et al. (2019) to compute the receiver bias. The satellite was obtained from the IONEX file of the University of Berne. We like to highlight here that in this file only satellite biases for GPS are provided. Therefore, we only compute absolute TEC for GPS data for comparison with the surrounding days. The further processing is done using dTEC for three reasons: first of all, because we wish to highlight the oscillatory behavior instead of the depletion caused by the eclipse; second, to be able to implement GLONASS data and improve the spatial coverage; third, to run the omega-k analysis as empty cells are simply set to zero which for dTEC means there is no variation whereas using absolute TEC, empty cells could cause artifacts.

To investigate the properties (wavelength and period) of the propagating TIDs during the eclipse, we apply the omega-k analysis developed by Eisenbeis et al. (2019). The omega-k analysis consists of detecting plane wave structures of the form $A_0 e^{-i(\boldsymbol{k}\cdot\boldsymbol{r}+\omega t)}$ in the space-time domain of the differential vTEC data set, where ω represents the wave's angular frequency which equals to $2\pi/T$, where T is the period of the wave, and $\boldsymbol{k}$ is the wave vector, which is the vector with a length equal to the wavenumber k in the direction perpendicular to the wavefronts. This means $|\boldsymbol{k}| = k = 2\pi/\lambda$. The direction of the wave vector $\boldsymbol{k}$ is ordinarily the direction at which the plane wave is traveling. This signal representation is adequate to detect the traveling waves signature by both measuring their characteristic temporal scale (period) as well as their physical extent (wavelength) in the considered region. For the computation of the omega-k analysis, we use the Fast Fourier Transform algorithm (Bracewell, 2000).

The omega-k analysis is performed on differential vTEC computed with a polynomial fit as described above. Note that no further filtering is performed, theoretically allowing the detection of low-frequency waves with periods larger than 1 hr. The discrete values for the angular frequency ω depend on the length of the total duration T_{length} of our differential vTEC data set and the sampling rate dt, where ω ranges from $-\pi/\text{d}t$ to $\pi/\text{d}t$ in steps of $2\pi/T_{\text{length}}$. The discrete values of the k-vector $\boldsymbol{k}(k_x, k_y)$ are described as follow: k_x depends on the size dlx of the cell in longitude and the size L_x of the whole grid's dimension in longitude; consequently, k_x ranges from $-\pi/\text{d}lx$ to $\pi/\text{d}lx$ in steps of $2\pi/L_x$. Following the same description, k_y depends on dly and Ly, respectively, the cell size and the whole grid's dimension in latitude. The ω and $\boldsymbol{k}(k_x, k_{y)}$ are related to period $T = 2\pi/\omega$ and wavelengths $\boldsymbol{\lambda}(\lambda_x, \lambda_y) = (2\pi/k_{x,}\ 2\pi/k_y)$ and expressed in minutes and km, respectively, to simplify the description of the observed TIDs.

In order to perform the omega-k analysis of the ionospheric signature of the eclipse, the differential vTEC is averaged and binned into a grid laid over South America. The size of the grid and the single cells vary in our study to show the robustness of the methodology. No interpolation is applied, so that cells without data are marked as blank. The blank cells are set to zero. Setting blank cells to zero implies that there's no variation of the TEC in that area. The 3D FFT is computed by doing a 1D Fast Fourier Transform along each dimension of the three-dimensional array. The TEC maps were created each 30 s for a period of 3 hr starting at 18:40 UTC which is 2 hr before the center of the eclipse first reaches Chile. The resulting 3D box of 2D TEC maps per 30 s over 3 hr is used as input for a 3D Fast Fourier Transform.

3. Results and Discussion

Difficulties identifying TEC depletions in TEC maps were encountered which may be related to either the sunset occurring directly after (or coinciding) with the total eclipse, or the short duration of totality upon reaching the South American continent. This supports the necessity of using the omega-k analysis to identify TIDs possibly related to the eclipse. Additionally, we find that the ionospheric region of totality is offset from the ground path of totality while the area of TEC depletion lags the eclipse and is located slightly north of the path of totality on the ground.

This is due to the eclipse geometry, which was illustrated and discussed by Verhulst and Stankov (2020). While we perceive the eclipse in visible wavelengths, the upper atmosphere is transparent to these wavelengths. The ionosphere reacts to a penumbra at XUV (X-ray and EUV) wavelengths, which predominantly originate at solar corona. The radius of the solar corona is 10%–25% larger than the photosphere, depending on the solar activity.

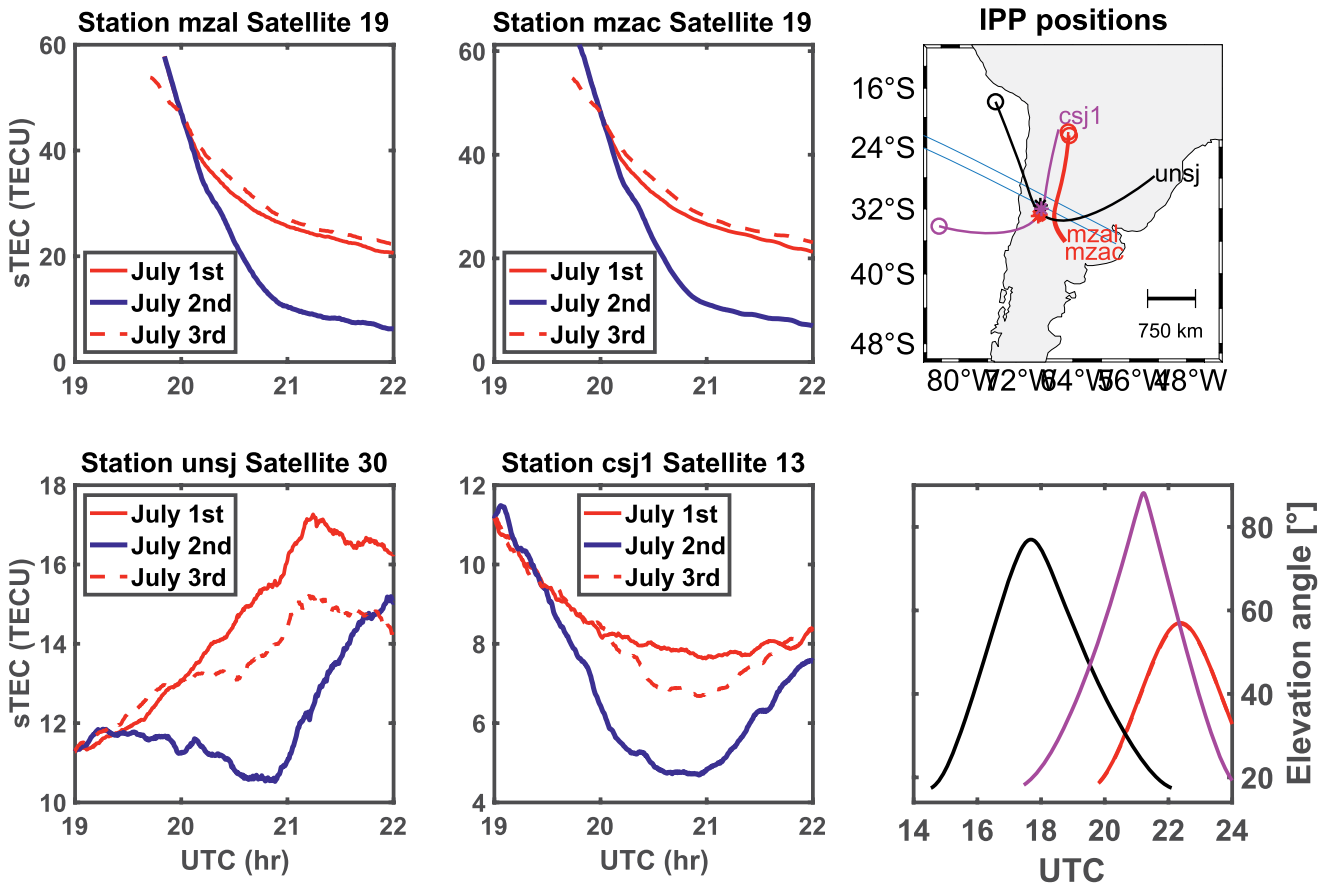


Figure 1. Top left and middle plots: absolute slant total electron content (sTEC) for stations MZAL (left) and MZAC (right) and Satellite 19 for the total solar eclipse (blue) and the surrounding days (red). Both stations lie in western Argentina where for the passing of Satellite 19 the eclipse acted like an early sunset. Bottom left and middle plots: Same absolute sTEC plots as above but for stations UNSJ (left) and CSJ1 (right) for Satellites 30 and 13. Right top plot: Time-space evolution of the IPPs for the station-satellite pairs shown in the four plots to the left. Same colors for same satellites: red for 19, black for 13, and magenta for 30. Positions of the stations (mostly colocated) is marked with an *, the start of the trajectory is marked with an o. Right bottom plot: Elevation angles of the satellite trajectories shown in the plot above.

Thus, there is no totality in the ionosphere. As already observed for the Great American Eclipse, the largest TEC depletion had a lag of about 10 min to the center of totality. Figure 1 shows the absolute sTEC for the South American Eclipse compared to the surrounding days. The four stations are all in the western part of Argentina within the path of totality and relatively close to the border with Chile. This is the part of South America that experienced the eclipse first, starting with 80% obscuration and the arrival of totality at approximately 20:40 UTC. In Figure 1, in the left and middle plots on the top, we can see a decrease in TEC starting around the time of the eclipse and reaching up to 15 TECU which resembles up to 40% of the background ionosphere of the surrounding days. In this case, the TEC also does not recover from the decrease as the end of the eclipse correlates with the sunset and therefore a lack of solar radiation to restore the state of the ionosphere prior to the eclipse. This is clearly visible for data from Satellite 19 used in Figure 1 where the eclipse acts in a way as an abrupt early sunset. In the left and middle bottom plots of Figure 1, we see a bit different behavior compared to the two stations using Satellite 19. In both cases, for station UNSJ and CSJ1 using Satellites 30 and 13, respectively, we see a depletion starting earlier and also the ionosphere recovering after the eclipse. We see a decrease of roughly 3–4 TECU which resembles 25%–40% of the background ionosphere of the surrounding days. This lies within the range of TEC decrease of 35% found by Jonah et al. (2020) for the same eclipse.

The plots on the right of Figure 1 show the time-space evolution of the IPPs for the four station-satellite combinations shown in Figure 1. For Satellite 19 (red lines), the satellite moves from the north right into the eclipse path and the signal stops when the satellite is a bit further south. This well explains the effect of the early sunset observed for those satellite-station pairs (Figure 1, top plots). For the two other satellite-station pairs where we

can see a recovery after the eclipse (Figure 1, bottom plots), the path of the satellite is moving through the path of totality but leaves it again on a northerly trajectory (black and magenta lines in Figure 1, right top). Therefore, we can see a recovery of the TEC after the eclipse for those two stations. For station UNSJ, the TEC increases even above the level observed before the eclipse which can be explained by the northbound trajectory of the chosen satellite and the increase in TEC in these regions due to the EIA and the enhanced plasma fountain (Bravo et al., 2020; Jonah et al., 2020).

We have applied the omega-k analysis to investigate the properties of the TIDs during the 2 July 2019 total solar eclipse in South America (Figure 3). We have used the method developed by Eisenbeis et al. (2019) for the Great American Eclipse. The main difference for the eclipse in South America is the less dense network of GNSS receivers and therefore less datapoints and the

smaller grid which means the resolution for the wavelength is not as good as for the Great American Eclipse. We have used different sized grids to compute the omega-k analysis to show that the results are robust even within those restrictions (Figure 2). The omega-k diagrams (on the top of Figure 2) for the two grids with different resolution clearly identify a zone of higher intensity for periods of 20–50 min and wavelengths over 200 km independently of the grid resolution. This correlates really well with the results of Eisenbeis et al. (2019) and Zhang et al. (2017) for the Great American Eclipse. This shows as well that our omega-k analysis also works well for data sets with less measurements and less dense GNSS networks. Although this influences the resolution of the results of the omega-k analysis, we can still clearly identify the TIDs induced by the TEC depletion due to the eclipse. In the two plots on the bottom, we cannot see this zone of higher intensity for the same period and wavelengths. The size of the grid used for the computation is in this case smaller with a northern limit of 24°S. This means the main TEC depletion caused by the eclipse north of the totality path on Earth is already on the edge or out of the grid. Therefore, we are not able to see the same intensity in these two cases. This also indicates that the TID is related to the TEC depletion due to the solar eclipse. In comparison with the day before (middle four plots in Figure 2) and the difference between the day of the eclipse and the day before, we can clearly identify a higher intensity in the zones associated with TIDs possibly associated with the eclipse. There are some areas of higher intensity for the day before the eclipse which might be related to geomagnetic activity as this was on the calming path of some days with higher geomagnetic activity. Notwithstanding this potential effect of the geomagnetic activity in the day before, the signals for the day of the eclipse are much stronger in intensity and therefore likely related to the eclipse itself. Our omega-k analysis highlights waves which are not easily visible in the space-time domain. In order to visualize the shape of those waves, in Figure 3, we show the identified TIDs with wavelength larger than 200 km and period of 20–50 min, as well as the TIDs with wavelength of 100–150 km and periods of <120 min, back in the space-time domain. Both TIDs are coherent with the position of the totality. Despite the presence of the TIDs is fully revealed, some bord effects could appear, in particular for the TIDs with period of 20–50 min and wavelength >200 km, and it shows the limit of the spectral method. Independently of the selected grid and resolution, the omega-k diagrams highlight the presence of TIDs with period of 20 to up to 120 min and wavelength of around 100 km also coherent with previous results.

Other than for the Great American Eclipse we cannot detect bow waves on this occasion. They are thought to be triggered by the supersonic speed of the shadow of the Moon and although for this eclipse the speed increases drastically for the part where it moves over land, covering the 1,300 km stretch across Argentina in 3 min which is a speed of ∼7 km/s compared to the maximum speed of 1.1 km/s for the Great American Eclipse, we find no evidence of high-frequency waves (10–20-min period). Bow waves have rather different origin and spatial morphology compared to the TEC depletion caused by the Moon's shadow itself. They do, however, have similar spectral characteristics although we are not able to detect any. In addition to the presence of the sunset, the generation of bow waves could also be suppressed by the direction of magnetic field lines, reducing the waves propagating southward.

4. Conclusion

A total solar eclipse occurred on 2 July 2019 over the Pacific Ocean and South America. Due to sparse or rather nonexistent coverage over the Pacific, we can only observe the last minutes of totality before sunset in Chile and Argentina. We see a clear decrease in TEC for the stations in western Argentina where the Moon's shadow first arrived over South America. Compared to the surrounding days those stations show a decrease of about 25–40%

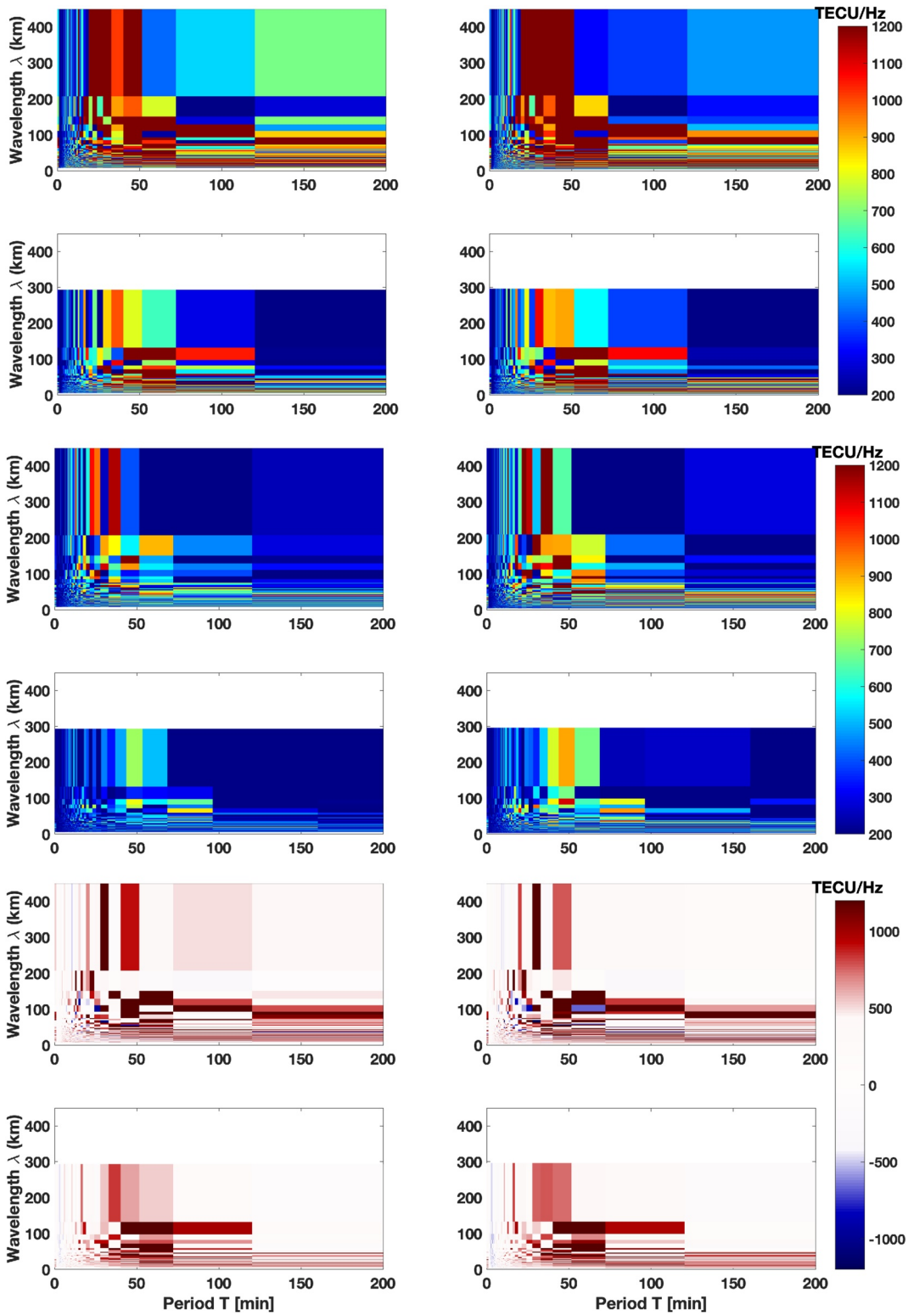


Figure 2. Top four plots, results of the omega-k analysis for the South American Eclipse. The diagrams show the wavelength over the period of the waves. Colors show the intensity for specific wavelengths and periods. We can clearly identify traveling ionospheric disturbances (TIDs) with a period of 20–50 min and a wavelength of >200 km for all different grids used. Displayed on the top are the results using a grid ranging from 74°W to 55°W in longitude and 40°S to 22°S in latitude, on the bottom from 72°W to 60°W in longitude and 36°S to 24°S in latitude. The number of cells varies from 40 in latitude and 70 in longitude for the plots on the left side to 140 cells in longitude and 70 cells in latitude for the right side. Middle four plots show the same results for the day before the eclipse and bottom four plots show the difference of the eclipse day and the day before the eclipse. Here, we can clearly highlight the TIDs with a wavelength >200 and <150 km for periods of 25–120 min.

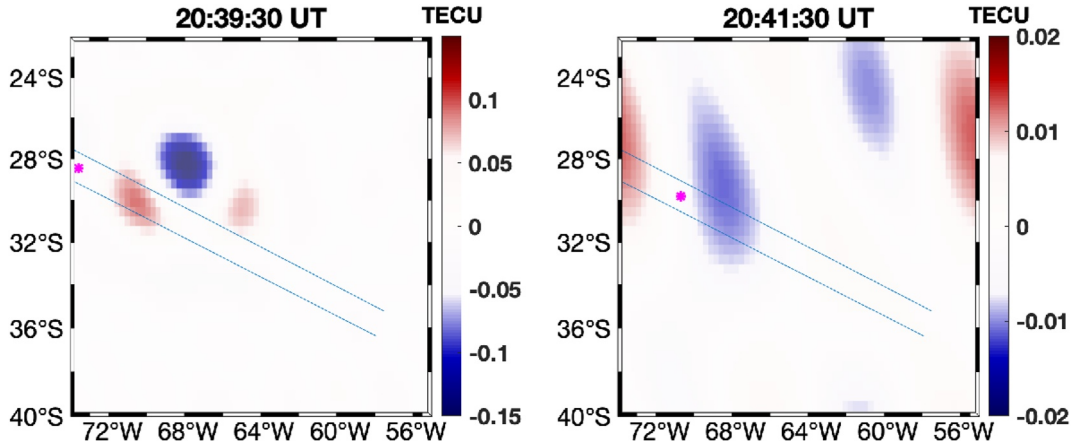


Figure 3. Right, identified traveling ionospheric disturbance (TID; period: 20–50 min, wavelength >200 km) back to the space-time domain (only the identified box in the omega-k diagram is sent back to space-time) for the larger grid with larger resolution (top left omega-k diagram). Results showed here are coherent with Figure 3 of Eisenbeis et al. (2019), related to the Great American Eclipse. Left, same as right plot but for the TID (period 25–120 min, wavelength <150 km).

compared to the background ionosphere. This lies within the expectations for solar eclipses at midlatitudes (Ding et al., 2010; Jakowski et al., 2008). Additionally, for GNSS station MZAL and MZAC—for which the IPPs moves further south in the path of the eclipse than the other stations shown—the TEC did not recover to the level before the arrival of the eclipse, this is because the eclipse coincided with sunset. This made it challenging to show the depletion due to the eclipse using differential TEC maps. Also, due to the low elevation angle of the Sun right before sunset, the Moon shadow at the ground does not necessarily coincide with the position of the shadow in the ionosphere. Therefore, the biggest effect is expected slightly north of the path of totality on Earth. Nevertheless, the implementation of GLONASS data improves the coverage, increasing the number of measurements by 1.5–2 times compared to GPS use only. By applying the omega-k analysis, we confirm the properties of the TIDs due to the TEC depletion induced by the eclipse. Both, the wavelength (around 100–150 and >200 km) as well as the period (20–50 min) correlates really well with results already obtained for the Great American Eclipse in August 2017 (Eisenbeis et al., 2019; Zhang et al., 2017). Additionally, we show the robustness of our methodology obtaining similar results for different grid resolution and sizes. The analysis of the TEC signature of the poorly covered South American eclipse observed by GNSS satellites in not propitious conditions (too close to the sunset) validates and generalizes our omega-k method to reveal the physical properties (period and wavelength) of generated traveling ionospheric disturbances (TIDs).

Data Availability Statement

This work was entirely based on freely available GNSS data from the following web resources: UNAVCO (www.unavco.org) and RAMSAC (http://www.ign.gob.ar).

Acknowledgments
We were grateful to the scientists and field technicians who have kept the GNSS networks in South America operational. This research was supported by the Programme National de Télédétection Spatiale (PNTS, http://programmes.insu.cnrs.fr/pnts/) Grant number PNTS-2020-16; by the CNES, granted project Global Ionospheric Seismology Network and Background; and by the Institut Universitaire de France (IUF). This was IPGP contribution 4190.

References

Afraimovich, E. L., Palamartchouk, K. S., Perevalova, N. P., Chernukhov, V. V., Lukhnev, A. V., & Zalutsky, V. T. (1998). Ionospheric effects of the solar eclipse of March 9, 1997, as deduced from GPS data. *Geophysical Research Letters*, *25*(4), 465–468. https://doi.org/10.1029/98GL00186

Bracewell, R. N. (2000). *The Fourier transform and its applications* (3rd ed.). McGraw Hill.

Bravo, M., Martínez-Ledesma, M., Foppiano, A., Urra, B., Ovalle, E., Villalobos, C., et al. (2020). First report of an eclipse from Chilean ionosonde observations: Comparison with total electron content estimations and the modeled maximum electron concentration and its height. *Journal of Geophysical Research: Space Physics*, *125*, e2020JA027923. https://doi.org/10.1029/2020JA027923

Cherniak, I., & Zakharenkova, I. (2018). Ionospheric total electron content response to the great American solar eclipse of 21 August 2017. *Geophysical Research Letters*, *45*, 1199–1208. https://doi.org/10.1002/2017GL075989

Coster, A. J., Goncharenko, L., Zhang, S.-R., Erickson, P. J., Rideout, W., & Vierinen, J. (2017). GNSS observations of ionospheric variations during the 21 August 2017 solar eclipse: GNSS TEC during 2017 solar eclipse. *Geophysical Research Letters*, *44*, 12041–12048. https://doi.org/10.1002/2017GL075774

Dautermann, T., & Calais, E. (2008). *TEC data processing software*. Purdue University.

Ding, F., Wan, W., Ning, B., Liu, L., Le, H., Xu, G., et al. (2010). GPS TEC response to the 22 July 2009 total solar eclipse in East Asia. *Journal of Geophysical Research*, *115*, A07308. https://doi.org/10.1029/2009JA015113

Eisenbeis, J., Occhipinti, G., Astafyeva, E., & Rolland, L. (2019). Short- and long-wavelength TIDs generated by the Great American Eclipse of 21 August 2017. *Journal of Geophysical Research: Space Physics*, *124*, 9486–9493. https://doi.org/10.1029/2019JA026919

Hoque, M. M., Wenzel, D., Jakowski, N., Gerzen, T., Berdermann, J., Wilken, V., et al. (2016). Ionospheric response over Europe during the solar eclipse of March 20, 2015. *Journal of Space Weather and Space Climate*, *6*, A36. https://doi.org/10.1051/swsc/2016032

Jakowski, N., Stankov, S. M., Wilken, V., Borries, C., Altadill, D., Chum, J., et al. (2008). Ionospheric behavior over Europe during the solar eclipse of 3 October 2005. *Journal of Atmospheric and Solar-Terrestrial Physics*, *70*(6), 836–853. https://doi.org/10.1016/j.jastp.2007.02.016

Jonah, O. F., Goncharenko, L., Erickson, P. J., Zhang, S., Coster, A., Chau, J. L., et al. (2020). Anomalous behavior of the equatorial ionization anomaly during the 2 July 2019 solar eclipse. *Journal of Geophysical Research: Space Physics*, *125*, e2020JA027909. https://doi.org/10.1029/2020JA027909

Le, H., Liu, L., Yue, X., Wan, W., & Ning, B. (2009). Latitudinal dependence of the ionospheric response to solar eclipses. *Journal of Geophysical Research*, *114*, A07308. https://doi.org/10.1029/2009JA014072

Lin, C. Y., Deng, Y., & Ridley, A. (2018). Atmospheric gravity waves in the ionosphere and thermosphere during the 2017 solar eclipse. *Geophysical Research Letters*, *45*, 5246–5252. https://doi.org/10.1029/2018GL077388

Lognonné, P., Artru, J., Garcia, R., Crespon, F., Ducic, V., Jeansou, E., et al. (2006). Ground-based GPS imaging of ionospheric post-seismic signal. *Planetary and Space Science*, *54*(5), 528–540. https://doi.org/10.1016/j.pss.2005.10.021

Momani, M. A., Yatim, B., & Mohd Ali, M. A. (2010). Ionospheric and geomagnetic response to the total solar eclipse on 1 August 2008 over Northern Hemisphere. *Journal of Geophysical Research*, *115*, A08321. https://doi.org/10.1029/2009JA014999

Mrak, S., Semeter, J., Drob, D., & Huba, J. D. (2018). Direct EUV/X-ray modulation of the ionosphere during the August 2017 total solar eclipse. *Geophysical Research Letters*, *45*, 3820–3828. https://doi.org/10.1029/2017GL076771

Mrak, S., Semeter, J., Nishimura, Y., Hirsch, M., & Sivadas, N. (2018). Coincidental TID production by tropospheric weather during the August 2017 total solar eclipse. *Geophysical Research Letters*, *45*, 10903–10911. https://doi.org/10.1029/2018GL080239

Piñón, D. A., Gómez, D. D., Smalley, R., Cimbaro, S. R., Lauría, E. A., & Bevis, M. G. (2018). The history, state, and future of the Argentine continuous satellite monitoring network and its contributions to Geodesy in Latin America. *Seismological Research Letters*, *89*(2A), 475–482. https://doi.org/10.1785/0220170162

Rideout, W., & Coster, A. (2006). Automated GPS processing for global total electron content data. *GPS Solutions*, *10*(3), 219–228. https://doi.org/10.1007/s10291-006-0029-5

Sun, Y., Liu, J., Lin, C. C., Lin, C., Shen, M., Chen, C., et al. (2018). Ionospheric bow wave induced by the moon shadow ship over the continent of United States on 21 August 2017. *Geophysical Research Letters*, *45*, 538–544. https://doi.org/10.1002/2017GL075926

Tsai, H. F., & Liu, J. Y. (1999). Ionospheric total electron content response to solar eclipses. *Journal of Geophysical Research*, *104*(A6), 12657–12668. https://doi.org/10.1029/1999JA900001

Verhulst, T. G. W., & Stankov, S. M. (2020). Height dependency of solar eclipse effects: The ionospheric perspective. *Journal of Geophysical Research: Space Physics*, *125*(7), e2020JA028088. https://doi.org/10.1029/2020JA028088

Zhang, S.-R., Erickson, P. J., Goncharenko, L. P., Coster, A. J., Rideout, W., & Vierinen, J. (2017). Ionospheric bow waves and perturbations induced by the 21 August 2017 solar eclipse. *Geophysical Research Letters*, *44*(2412), 12067–12073. https://doi.org/10.1002/2017GL076054